PAPER

Columnar liquid crystalline triphenylene-bis(dithiolene)nickel complexes. Soft photothermal materials†

Silvia Cobos, [a] Gregorio García, [a] César L. Folcia, [b] Josu Ortega, [b] Jesús Etxebarria, *[b] Gabriel López-Peña, [c] Dirk H. Ortgies, [de] Emma Martín Rodríguez [ce] and Silverio Coco *[a]

This work reports new soft photothermal materials based on liquid crystalline nickel bis(dithiolene) complexes bearing pentakis(dodecyloxy)triphenylene units in which the triphenylene core and the metal complex are linked through $-(CH_2)_n-$ (n = 2, 4, 10) connectors. The mesomorphic properties of these materials can be modulated by the length of the linker. All the complexes, except the derivative with the longest linker, show columnar mesomorphism, characterized by polarized optical microscopy (POM), differential scanning calorimetry (DSC) and X-ray scattering studies. The structure of the mesophases contains segregated organic and inorganic columns supported respectively by π-stacking of the triphenylene discs and weak intermolecular nickel–sulfur interactions. The photothermal activity was studied on the complex with n = 2. Under laser irradiation with a power density of 0.098 W cm^{-2} for just over a minute an increase in temperature of ΔT = 50 °C was achieved. This produced the melting of the crystalline solid to give rise to the columnar mesophase, where, interestingly, the photothermal effect was enhanced. Quantum chemical calculations have also been performed to gain insight into the supramolecular self-assembled columnar structure at the molecular level, as well as into the photothermal behavior.

Introduction

Discotic liquid crystals (DLCs) are a fascinating group of soft self-assembled materials that possess adequate electronic features for a wide range of applications, including organic light-emitting diodes, field effects transistors, conductive devices, photovoltaic cells,[1–3] liquid-crystal displays[4,5] and biosensors.[6] DLCs typically form columnar mesophases in which intermolecular interactions, such as van der Waals forces, electrostatic interactions, π–π stacking or hydrogen bonds promote the supramolecular columnar organization.[2]

Thiphenylene-based mesogens are among the most widely studied columnar liquid crystals,[7,8] their properties can be tuned by tailoring the triphenylene core with a great diversity of functional groups,[9–17] including metal complexes.[18–26] When such functionalization is carried out at one end of the side chains of triphenylene, the triphenylene core and the functional group tend to self-assemble individually, leading to the formation of mesophases with segregated columns of different nature, which offers many opportunities to modulate the properties of the system.[27–35] In this regard, our group has reported hybrid organic/inorganic multicolumnar mesophases containing triphenylene moieties,[36,37] where luminescence,[38] charge transport along the columnar stacking,[39,40] and thermochromism,[41] are easily modulated by the metal fragment.

Photothermal materials, which absorb light, particularly in the near infrared region (NIR), and convert it into thermal energy,[42] are also promising functional materials for multiple applications in fields such as phototherapy,[43–45] photocatalysis,[46–48] heaters[49,50] or solar energy generation.[51] These materials can be designed for a variety of systems

[a] IU CINQUIMA/Química Inorgánica, Facultad de Ciencias, Universidad de Valladolid, 47071 Valladolid, Castilla y León, Spain. E-mail: silverio.coco@uva.es

[b] Department of Physics, University of the Basque Country, UPV/EHU, 48080 Bilbao, Spain. E-mail: j.etxeba@ehu.es

[c] Departamento de Física Aplicada, Universidad Autónoma de Madrid, C/Francisco Tomás y Valiente 7, 28049, Madrid, Spain

[d] Departamento de Física de Materiales, Universidad Autónoma de Madrid, C/ Francisco Tomás y Valiente 7, 28049, Madrid, Spain

[e] Nanomaterials for BioImaging Group, Instituto Ramón y Cajal de Investigación Sanitaria IRYCIS, Ctra. de Colmenar km 9, 300, 28034, Madrid, Spain

† Electronic supplementary information (ESI) available: Materials and methods, full details of synthetic methods, spectroscopic and analytical data for the new compounds, DSC thermograms and X-ray diffraction patterns not included in the text. See DOI: https://doi.org/10.1039/d4tc01338g

12332 | *J. Mater. Chem. C,* 2024, **12**, 12332–12340

This journal is © The Royal Society of Chemistry 2024

including metallic nanostructures, inorganic semiconductors, carbon-based materials and polymers.[45] In the soft nanotechnology field, incorporation of photothermal systems into matrices of soft materials, for example liquid crystals,[52] constitutes an emerging approach to realize advanced and tunable materials with enhanced properties for high-tech applications.

Seeking thermotropic liquid crystals based on metal complexes that can induce metal-centered photothermal properties without the need of composites, our attention turned to triphenylene nickel bis(dithiolene) complexes. It is known that these complexes exhibit high thermal stability, photostability and photothermal activity,[53,54] and are good platforms for designing metallomesogens.[55–57]

In this work we report examples of mesomorphic nickel bis(dithiolene) complexes derived from triphenylene, which display high photothermal activity. The structure of the mesophase contains segregated organic and inorganic columns supported respectively by π-stacking of the triphenylene discs and weak intermolecular nickel–sulfur interactions. In addition, quantum chemical calculations have also been performed to gain insight into the supramolecular self-assembled columnar structure at the molecular level, as well as into the photothermal behavior.
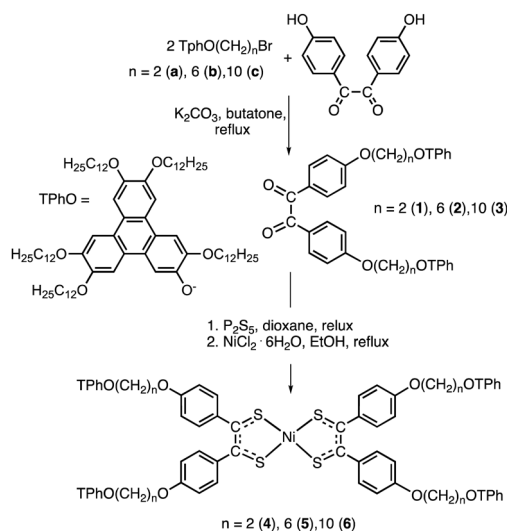
Results and discussion

Synthesis and characterization

The synthesis of the new nickel-bis(dithiolene) complexes was carried out starting from 4,4′-dihydroxybenzil, according to Scheme 1, as described for related nickel complexes.[56,57] The complexes were isolated as dark-green powders.

Elemental analyses, yields, high-resolution mass spectra, and relevant IR and NMR characterization data for the complexes are given in the experimental section (ESI†).

The nickel complexes show well-resolved ^{1}H and ^{13}C{^{1}H} NMR spectra, consistent with square-planar diamagnetic molecules. This correlates well with the fact that in the X-ray crystal structures
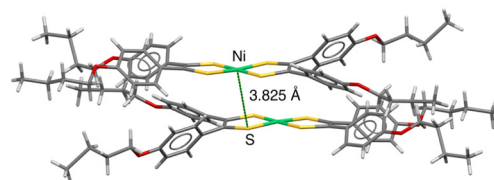

Fig. 1 Crystal packing for 1,2-bis-(4-butoxyphenyl)ethylene-1,2-dithiolene nickel complex from single crystal X-ray diffraction data.[58]

of similar 1,2-bis-(4-alkoxyphenyl)ethylene-1,2-dithiolene complexes without the triphenylene group (reasonable models to 4–6), the nickel atom has an essentially perfect square-planar environment (Fig. 1).[58] The solid-state arrangement is characterized by a clear segregation of the alkyl chains. The molecules are stacked in a parallel disposition, but each molecule is slightly shifted from the previous one (Fig. 1). The shortest intermolecular distances observed between neighboring molecules correspond to Ni···S distances of 3.825 Å. This distance would exclude the existence of any significant covalent Ni···S interactions.

The UV-Vis absorption and fluorescence data of the benzil precursors (1–3) and the nickel complexes (3–6) in dichloromethane solution are summarized in Table S1 (ESI†).

The electronic absorption spectra of the substituted benzils are all very similar (Fig. 2 and Table S1, ESI†), displaying a very structured spectral pattern with very intense absorption bands typical of 2,3,6,7,10,11 hexaalkoxytriphenylenes.[59,60] In the compounds reported here, the triphenylene and the benzil group (nickel moieties in the complexes) are not electronically connected. Thus, as experimentally observed, significant influence on its electronic transitions is not expected.[36,37,39,40] For the nickel complexes, in
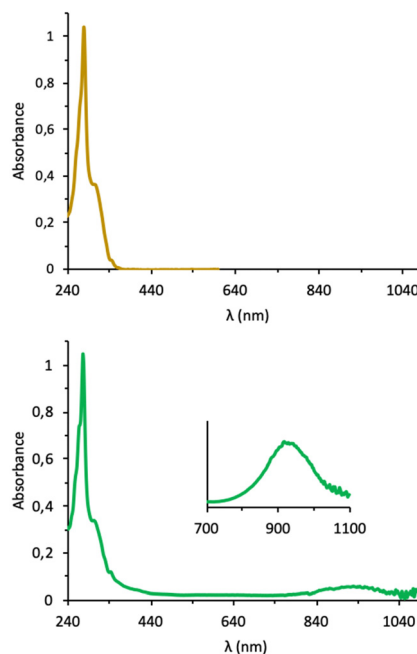

Scheme 1 Synthesis of nickel bis(dithiolene) complexes.

Fig. 2 UV-Visible spectra of the benzil precursor 1 (top) and its nickel complex 4 (bottom) in dichloromethane (2 × 10^{-6} M) at 298 K. The magnified region is from a 2.5 × 10^{-5} M solution.

This journal is © The Royal Society of Chemistry 2024

J. Mater. Chem. C, 2024, 12, 12332–12340 | 12333

addition to the absorption bands from the triphenylene groups, the electronic spectra show one broad absorption band in the NIR (Fig. 2) at λ_{max} = 918–922 nm, which in similar complexes but without triphenylene groups, is assigned to $\pi \rightarrow \pi^*$ transitions involving dithiolene-based orbitals (HOMO → LUMO).[58,61]

Density functional theory (DFT) calculations were carried out in order to confirm the nature of the electronic absorptions in our system (see (ESI†)). The vertical excitation energies (ΔE_{TD}), oscillator strengths (f) and nature (defined as the main contribution) of the main electronic transitions are reported in Table 1. In the high energy region, the electronic transition at 291 nm (experimental value 277 nm) is identified as the HOMO-4 → LUMO+4 transition with a 95% contribution. Both HOMO−4 and LUMO+4 molecular orbitals are over triphenylene fragment. The other two electronic transitions at 311 nm and 938 nm (experimental values 306 nm and 922 nm, respectively) arise from the Ni-bis(dithiolene) core. The absorption peak in the NIR region (calculated at 938 nm) is due to the HOMO → LUMO transition with a 96% contribution.

As for their luminescence spectra, all the emission spectra in dichloromethane solution are similar (Fig. 3), and analogous to those of 2,3,6,7,10,11-hexaalkoxytriphenylenes.[60,62] As observed frequently in triphenylene derivatives,[38,39] the luminescence is lost in the solid state and in the mesophase.

Thermal behavior and self-organization properties

The mesomorphic properties have been studied using polarized optical microscopy (POM), differential scanning calorimetry
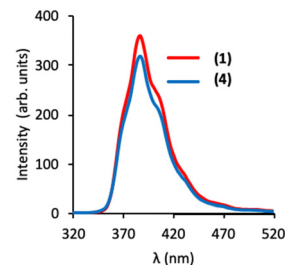

Fig. 3 Luminescence emission spectra of the benzil precursor **1** and its nickel complex **4** in dichloromethane solution at 298 K (λ_{exc} = 278 nm).

(DSC), and X-ray scattering. The optical, thermal and thermodynamic data are collected in Table 2. Representative microphotographs are shown in Fig. 4. Regarding the thermal stability of the compounds studied, thermogravimetric analysis performed in a thermobalance by heating it up to 800 °C under N_2 shows a good thermal stability up to temperatures above 250 °C (Fig. S52–S54 of the ESI†).

For the benzil precursors, only the derivative with the shortest connection between the triphenylene core and the benzil group ($n = 2$) displays liquid crystal behavior, being monotropic in nature. However, we have not been able to identify the mesophase. In contrast, all the nickel compounds, except complex 6 that is not a liquid crystal, show enantiotropic mesomorphism at temperatures close to ambient. Thus, the formation of nickel bis(dithiolene) complexes helps the appearance of mesomorphism in these systems. Most likely, this is due to the fact that in the metal complexes

Table 1 Calculated excitation energies (ΔE_{TD}), oscillator strengths (f) and main configurations of **4** in dichloromethane solvent computed at CAM-B3LYP-D3BJ/6-31 + G(d,p)/Def2-TZVP using sTDA approach

ΔE_{TD} (nm)	f	Configuration[ab]		Experimental (nm)[c]
		HOMO-4	LUMO+4 (95)	
291	0.2106		→	277
		HOMO	LUMO+2 (93)	
311	0.2596		→	306
		HOMO	LUMO (96)	
938	0.1069		→	922

[a] Percentage contribution in parentheses. [b] The shape of the implied molecular orbitals is also displayed (isosurface value 0.03 a.u.) along to their corresponding energies calculated at CAM-B3LYP/6-31 + G(d,p)/Def2-TZVP in dichloromethane solvent. Hydrogen atoms are omitted. [c] Experimental values in dichloromethane.

12334 | *J. Mater. Chem. C*, 2024, **12**, 12332–12340

This journal is © The Royal Society of Chemistry 2024

Table 2 Optical, thermal, and thermodynamic data for the benzil precursors and their nickel-bis(dithiolene) complexes

Cpd	Transition[a]	T^b (°C)	ΔH^b (kJ mol^{-1})
1	Cr → Cr′[c]	29	19.0
	Cr → I[c]	69	86.6
	I → M	68	4.0
	M → Cr′	57	1.2
	Cr′ → Cr	15	17.2
2	Cr → I	59	75.6
3	Cr → I[c]	50	95.7
4	Cr → Col$_{rec}$	56	32.0
	Col$_{rec}$ → I	127	14.2
5	Cr → Cr′	5	50.1
	Cr′ → Col$_{rec}$	35	36.2
	Col$_{rec}$ → I	107	23.2
6	Cr → I[c]	36	126.0

[a] Cr, crystal phase; M, unidentified mesophase; Col$_{rec}$, rectangular columnar mesophase; I, isotropic liquid. [b] Data collected from the second heating DSC cycle. The transition temperatures are given as peak onsets. [c] Data collected from the first heating DSC cycle. Complex transitions below melting points have been omitted for clarity. All the DSC scans registered from −40 °C can be found in the Electronic ESI.
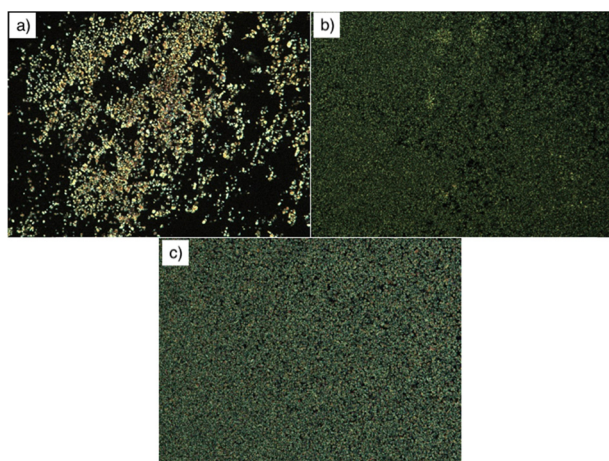

Fig. 4 Optical polarizing microscopy photographs (×100, crossed polarizers) on cooling from the isotropic phase of: (a) benzil precursor (1) at 67 °C; (b) nickel complex 4 at 109 °C; (c) nickel complex 5 at 119 °C.

the number of triphenylenes per molecule is duplicated with respect to the benzil precursors, which improves the balance of favorable enthalpic interactions (attractive π–π stacking contributions from four triphenylene core per molecule) *versus* unfavorable entropic contributions into a columnar stacking.

In all cases, the transition temperatures decrease with the increasing length of the connector chain between the triphenylene core and the metal moiety.

The textures observed by POM on cooling from the isotropic liquid are similar for all compounds and show mosaic-like textures, which are consistent with the presence of columnar mesomorphism. This was confirmed by X-ray studies.

X-ray scattering studies.

X-ray studies were carried out on powder samples using a diffractometer with an attachment for temperature control

(see ESI† for the experimental details). We will present the results for compounds **1**, **4** and **5** which are the materials showing mesophases.

The X-ray pattern of **1** at the isotropic liquid (I) phase (Fig. S55 of the ESI†) shows two broad peaks, one of them at 4.5 Å ($2\theta \sim 20°$), which corresponds to the molten chains in liquid disorder, and another one at small angles at $2\theta \sim 4°$ (20 Å) representative of the molecular geometry. The transition to the mesophase is observed on cooling below 68 °C. The low-angle reflection of the diagram at the I phase sharpens considerably and splits into two (Fig. 5). At 60 °C the corresponding spacings are 23.3 Å and 32.7 Å. With only two reflections no reliable information could be obtained about the type of mesophase although, given the molecular shape, it is likely to be a columnar liquid crystal. However, no signs of molecular stacking in columnar organization could be detected in the diagram at wide angles, which remained unaltered. Upon further cooling two crystalline phases were observed as shown in Fig. S56 of the (ESI†).

Compound 4 shows a diagram similar to that of the preceding compound at the I phase (Fig. S57 of the ESI†) but the pattern at the mesophase is considerably richer (Fig. 6).

The low-angle reflections could be indexed satisfactorily by assuming a Col$_{rec}$ structure. The lattice is centered and the plane group is $c2mm$, which has the maximum symmetry of the orthorhombic plane groups. The lattice parameters are a = 79.5 Å and b = 55.9 Å. In the wide-angle region, apart from the diffuse halo at 4.5 Å, a sharper weak reflection is observed at $2\theta = 24°$ (3.6 Å). This spacing is likely to be connected to the stacking distance between triphenylene groups, which transmit their columnar organization to the rest of the molecular fragments. With this stacking distance the resulting mass density is $\sigma = 1.1$ g cm^{-3} if we suppose $Z = 2$ molecules per unit cell. A possible electronic density map obtained from the intensities of the peaks in Fig. 6(a) is shown in Fig. 7. The solution for the map is not unique since there are many relevant peaks involved, parts of the maps we found have very similar characteristics. (See the ESI† for an explanation of the procedure for obtaining the charge density maps). In the map of Fig. 7 two molecules per cell can be appreciated, with 4 triphenylene groups surrounding the metal fragment, which has the highest
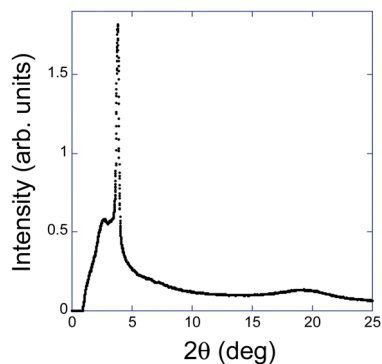

Fig. 5 X-ray pattern of **1** at the mesophase (60 °C).

This journal is © The Royal Society of Chemistry 2024

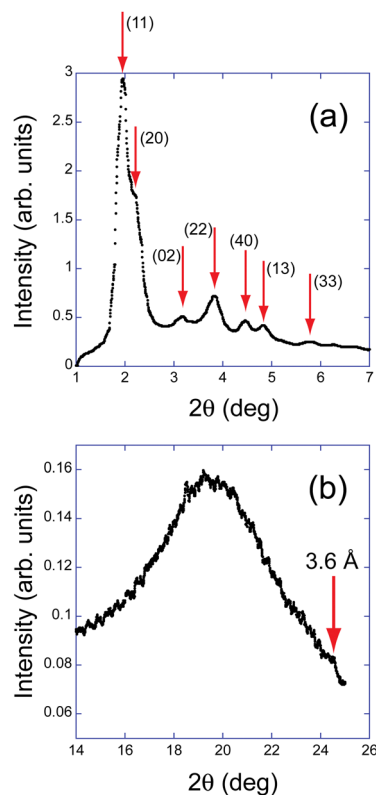*J. Mater. Chem. C*, 2024, **12**, 12332–12340 | **12335**

Fig. 6 X-ray patterns at the small-angle (a) and wide-angle (b) regions of **4** at 60 °C. The small-angle reflections are indexed assuming a Col$_{rec}$ phase of parameters $a = 79.5$ Å and $b = 55.9$ Å. A stacking distance along the columns $h = 3.6$ Å can be glimpsed as a small peak at the wide-angle region.
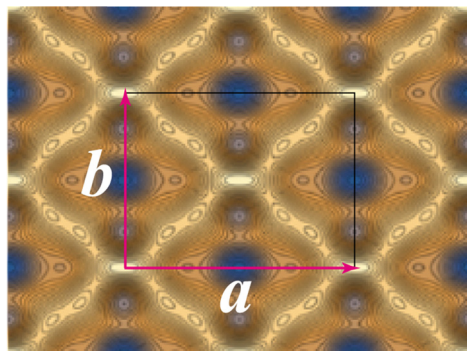

Fig. 7 Electronic density map of **4** at 60 °C. The brighter areas represent larger electronic densities. The symmetry of the map is $c2mm$ and the unit cell parameters a and b are sketched.

electronic density. The empty space is filled with alkyl chains, with lower electronic density.

Fig. 8(a) and (b) show the low-angle and wide-angle regions of the X-ray pattern of **5** measured at 80 °C.

Again, the peaks at low angles are well indexed with a centered Col$_{rec}$ phase, with cell parameters $a = 79.0$ Å and $b = 68.3$ Å. In this compound the stacking distance along the columns, $h = 3.56$ Å, is clearly visible. This peak could be easily
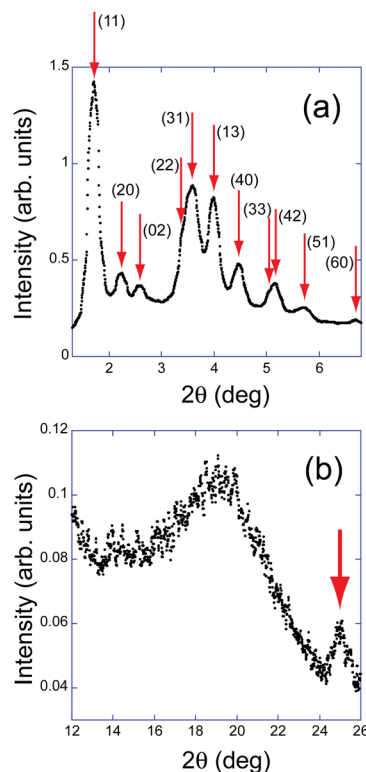

Fig. 8 X-ray patterns at the small-angle (a) and wide-angle (b) regions of **5** at 80 °C. The small-angle reflections are indexed assuming a Col$_{rec}$ phase of parameters $a = 79.0$ Å and $b = 68.3$ Å. A stacking distance along the columns $h = 3.56$ Å is clearly visible as a well-defined peak at the wide-angle region.

followed in the whole mesophase range and it was found that h shows a slight temperature dependence (see Fig. S58 of the ESI†). The mass density at 80 °C is $\sigma = 0.96$ g cm^{-3} assuming $Z = 2$ molecules per unit cell. Fig. 9 shows the electronic density map calculated from the data of Fig. 8(a). The symmetry of the map is again $c2mm$. The brightest regions at the center and vertices of the cell indicate the positions of the metal-containing molecular fragments and the secondary maxima (4 per molecule) the triphenylene locations.
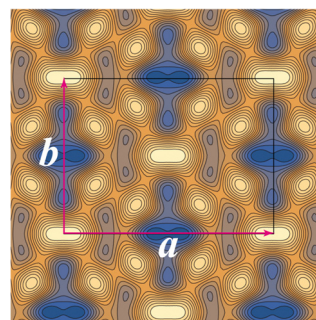

Fig. 9 Electronic density map of **5** at 80 °C. The brighter areas represent higher electron densities. The unit cell parameters a and b are also sketched. Two molecules per cell are identified through the positions of the main (metal segments) and secondary (triphenylenes) maxima.

12336 | J. Mater. Chem. C, 2024, **12**, 12332–12340

This journal is © The Royal Society of Chemistry 2024

For the sake of completeness, we give in the ESI† the X-ray patterns of the I phase (Fig. S59 of the ESI†) and the two crystalline phases (Fig. S60 of the ESI†) of compound **5**.

Photothermal activity

The presence of a NIR absorption band prompted us to explore the photothermal activity of the bis(dithiolene) complexes. Since the characteristic absorption wavelength of the bis(dithiolene) core remains largely unchanged when modifying the distance between the two electronically independent fragments (*i.e.*, triphenylene and metal–organic center), our efforts have been focused on **4**, chosen as a representative complex.

The increase in temperature (ΔT) of the nickel complex in the solid state was measured under laser irradiation (980 nm) with three different laser power densities (0.024, 0.060 and 0.098 W cm^{-2}) for 4 min. Fig. 10 shows the thermal camera images of the maximum temperatures that the sample reached for the three different power densities. In particular, after irradiating the samples with a 980 nm laser at 0.024, 0.060 and 0.098 W cm^{-2}, the sample reached temperatures of 35.5, 56.1 and 76.6 °C, respectively. Moreover, 2 control experiments were performed. First an empty plastic tube was exposed to 980 nm laser excitation at the maximum power density (0.098 W cm^{-2}) to exclude any influence of the tube's polymer on the heating process. The maximum temperature of 20.8 °C stayed at room temperature and thereby demonstrated that all observable temperature increase was a consequence of the nickel complex. The 2nd control was performed at 690 nm, a wavelength in a non-absorbing region of the compound, and 0.098 W cm^{-2} resulting in a maximum temperature of 21.3 °C, respectively, which can be considered as negligible photothermal behavior in comparison.

Fig. 11 shows the heating and cooling curves of the studied sample, irradiating with a 980 nm laser at the previously mentioned power densities. In all three cases a clear photothermal effect was observed. Under laser irradiation with a power density of 0.098 W cm^{-2} for 4 min, an increase in temperature of $\Delta T = 56.6$ °C was measured. However, it should be noted that for just over a minute of irradiation an increase in temperature of $\Delta T = 50$ °C had already been achieved. In
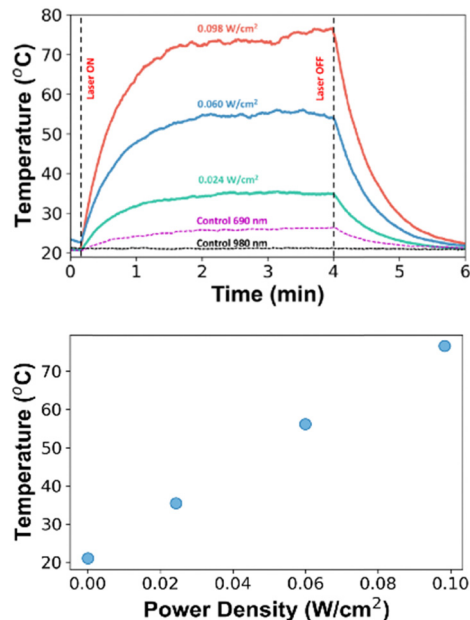

Fig. 11 Top: Heating and cooling curves after 980 nm laser irradiation. The control curves for 980 and 690 nm laser irradiation are included; Bottom: Maximum temperature reached *versus* power density with 980 nm irradiation.

addition, after three minutes at the maximum intensity of radiation (Fig. 11(top)), a clear increase in the photothermal behavior was detected at a temperature slightly above 70 °C, where the compound should be transiting into the mesophase. Noting that, the phase transition temperatures deduced from photothermal measurements may be slightly shifted with respect to the DSC data (Table 2) due to the different heating ramps and the different experimental techniques used, in which phase transitions may naturally show up at moderately different temperatures.

Therefore, the strong photothermal behavior of this system, which increases the temperature up to a maximum of 77 °C under 980 nm laser excitation, produces the melting of the solid phase to give rise to the columnar mesophase, where the photothermal effect is enhanced.

Quantum chemical calculations

Quantum chemical calculations were carried out to gain a deeper insight into one-dimensional columnar structure in the mesophase, as well as the electronic absorption properties at the molecular level. Firstly, the columnar structure in the mesophase was described through a cluster of four molecules (which entails 1108 atoms) stacked along *z*-axis (see ESI† for more details). Fig. 12 displays the optimized supramolecular structure with a length connector between the triphenylene core and the nickel complex of two carbons. Additionally, an analysis on the intermolecular interactions using reduced density gradient (RDG) isosurfaces is provided.[38]

As seen in Fig. 12, the molecules are stacked on top of each other along the *z*-axis, which is perpendicular to the plane containing the central organometallic complex. Additionally,
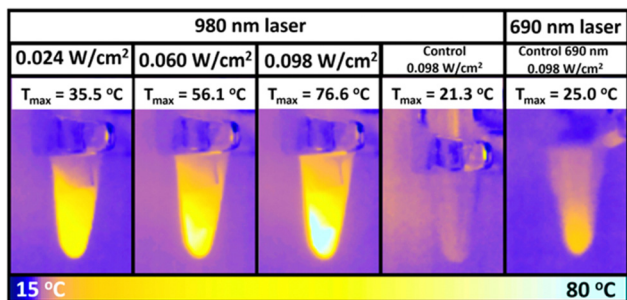

Fig. 10 Thermal camera images at the maximum temperature reached for irradiations at 980 nm and 690 nm. The image includes the control experiments irradiated at 980 and 690 nm for the maximum used power density (0.098 W cm^{-2}).

This journal is © The Royal Society of Chemistry 2024

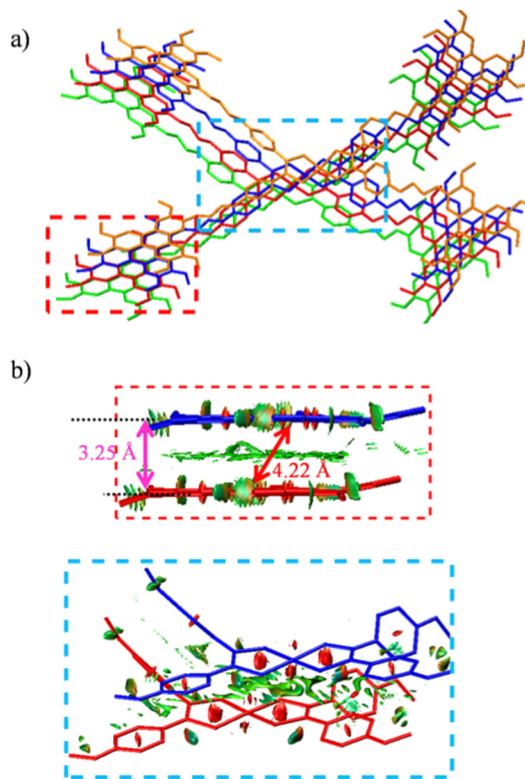*J. Mater. Chem. C*, 2024, **12**, 12332–12340 | **12337**

Fig. 12 (a) Upper view of the minimum-energy structure of a tetramer cluster of **4** optimized at the GFN2-xTB level. Each molecule is shown in a different color. H atoms are omitted. (b) Analysis of non-covalent interactions through RDG isosurfaces, with a focus on the interactions between two central molecules. Green regions represent van der Waals interactions. For clarity, RDG isosurfaces are only shown for one organic column and the organometallic region.

there is a lateral displacement along the xy plane. As previously noted, the main characteristic of this columnar phase, is the micro-segregation between organic and organometallic fragments in different columnar regions. Thus, within each organic or organometallic region, triphenylene or Ni-organometallic fragments are parallelly stacked. However, for each molecule, the planes containing the triphenylene units on opposite sides are staggered between them and twisted with respect to the metal–organic moiety, with dihedral angles of approximately $40°$. Within the organic column, green RDG isosurfaces between triphenylene motifs and the intermolecular distances between them, $d_{(TPh–TPh)} = 3.3$ Å (measured as the shortest distance between TPh planes) indicating π-stacking interactions between them. Regarding the interactions between the organometallic fragments, the green RDG isosurfaces between them indicate van der Waals interactions, with distances $d_{(C–S)} \sim 3.6$ Å (measured as the shortest intermolecular distance between C and S atoms parallel to the z-axis). The lateral displacement between molecules promotes the formation of Ni$\cdots$S interactions (denoted by the presence of green RDG isosurfaces between Ni and S atoms), with a $d_{(Ni\cdots S)} \sim 3.5$ Å, which is shorter than those found in the X-ray structures. This supports that the melting of the crystals produces a slippage of the metal fragments reducing the Ni$\cdots$S intermolecular

distances. Therefore, π-stacking interactions promote the formation of the organic column, while the organometallic column is stabilized by Ni$\cdots$S interactions.

Subsequently, based on the above optimized structure, we assessed electronic absorption features by computing vertical electronic excitation energies, with emphasis on the NIR region. Vertical electronic excitation energies were calculated using an ONIOM embedding model in conjunction with sTDA (see ESI† for more details). Our results display that in the columnar structure, electronic absorption in the NIR region is similar to that found in solution, and predominantly arises from an intramolecular process. Furthermore, the inclusion of more than one molecule (to account for intermolecular interactions between organometallic fragments) is adequate for an accurate description of the NIR absorption features. In agreement with experimental data obtained from a thin film of the supercooled mesophase at room temperature (Fig. S64 of the ESI,† $\lambda_{max} = 884$ nm), there is a transition in the NIR region with $\Delta E_{TD} = 879$ nm, which is attributed to a HOMO $\rightarrow$ LUMO one-electronic transition (with a 96% contribution), with both orbitals located over the Ni-bis(dithiolene) core.

Conclusions

This study shows that the chemical functionalization of substituted triphenylenes at the end of one of the alkoxy substituents with a nickel-dithiolene synthon, which strong photothermal response is known, constitutes a simple and useful strategy to design efficient photothermal columnar mesophases. The mesomorphic properties of these materials can be modulated by the length of the alkyl chain that act as linker between the triphenylene core and the nickel complex. As the length of that spacer increases, the intermolecular interactions weaken and the transition temperatures decrease, until liquid crystal behavior is lost. The mesomorphic complexes display uncommon columnar mesophases that contain segregated organic and inorganic columns that are supported respectively by π-stacking of the triphenylene discs and weak intermolecular nickel–sulfur interactions.

The nickel complexes display one broad absorption band in the near-IR (NIR) region, which is characteristic of the bis(dithiolene) fragment, and independent of the length of the spacer used. The photothermal activity of this system was studied on the complex **4**. It displays a strong photothermal effect that produces the melting of the crystalline solid to give rise to the columnar mesophase, where, interestingly, the photothermal effect is enhanced. These results reveal the great potential of metal–organic molecules as photothermal soft materials for new applications. For example, these materials could not only be used as converters of light energy into heat, but also as phase change materials for thermal storage.

Author contributions

The authors have contributed equally to the paper.

12338 | *J. Mater. Chem. C*, 2024, **12**, 12332–12340

This journal is © The Royal Society of Chemistry 2024

Data availability

The authors declare that the data supporting this article have been included as part of the ESI.†

Conflicts of interest

There are no conflicts to declare.

Acknowledgements

References

1 T. Kato, N. Mizoshita and K. Kishimoto, *Angew. Chem., Int. Ed.*, 2006, **45**, 38.

2 R. De, S. Sharma, S. Sengupta and S. Kumar Pal, *Chem. Rec.*, 2022, e202200056.

3 H. K. Bisoyi and Q. Li, *Chem. Rev.*, 2022, **122**, 4887.

4 H. Mori, Y. Itoh, Y. Nishiura, T. Nakamura and Y. Shinagawa, *Jpn. J. Appl. Phys.*, 1997, **36**, 143.

5 H.-W. Chen, J.-H. Lee, B.-Y. Lin, S. Chen and S.-T. Wu, *Light: Sci. Appl.*, 2018, **7**, 17168.

6 Z. Wang, T. Xu, A. Noel, Y.-C. Chen and T. Liu, *Soft Matter*, 2021, **17**, 4675.

7 S. Kumar, S. Setia, B. S. Avinash and S. Kumar, *Liq.Cryst.*, 2013, **40**, 1769.

8 T. Wöhrle, I. Wurzbach, J. Kirres, A. Kostidou, N. Kapernaum, J. Litterscheidt, J. H. Haenle, P. Staffeld, A. Baro, F. Giesselmann and S. Laschat, *Chem. Rev.*, 2016, **116**, 1139.

9 N. Boden, R. J. Bushby and A. N. Cammidge, *Liq. Cryst.*, 1995, **18**, 673.

10 N. Boden, R. J. Bushby, A. N. Cammidge and G. Headdock, *J. Mater. Chem.*, 1995, **5**, 2275.

11 S. Kumar, M. Manickam, V. S. K. Balagurusamy and H. Schonherr, *Liq. Cryst.*, 1999, **26**, 1455.

12 R. J. Bushby, N. Boden, C. A. Kilner, O. R. Lozman, Z. Lu, Q. Liu and M. A. Thornton-Pett, *J. Mater. Chem.*, 2003, **13**, 470.

13 N. Boden, R. J. Bushby, Z. B. Lu and A. N. Cammidge, *Liq. Cryst.*, 1999, **26**, 495.

14 K. Praefcke, A. Eckert and D. Blunk, *Liq. Cryst.*, 1997, **22**, 113.

15 N. Boden, R. J. Bushby, A. N. Cammidge, S. Duckworth and G. Headdock, *J. Mater. Chem.*, 1997, **7**, 601.

16 N. Boden, R. J. Bushby, A. N. Cammidge and G. Headdock, *Synthesis*, 1995, 31.

17 S. Kumar, M. Manickam, S. K. Varshney, D. S. S. Rao and S. K. Prasad, *J. Mater. Chem.*, 2000, **10**, 2483.

18 S. Kumar and S. K. Varshney, *Liq. Cryst.*, 2001, **28**, 161.

19 J. L. Schulte, S. Laschat, R. Schulte-Ladbeck, V. von Arnim, A. Schneider and H. Finkelmann, *J. Organomet. Chem.*, 1998, **552**, 171.

20 A. N. Cammidge and H. Gopee, *Chem. Commun.*, 2002, 966.

21 B. Mohr, G. Wegner and K. Ohta, *Chem. Commun.*, 1995, 995.

22 F. Yang, X. Bai, H. Guo and C. Li, *Tetrahedron Lett.*, 2013, **54**, 409.

23 J. Shi, Y. Wang, M. Xiao, P. Zhong, Y. Liu, H. Tan, M. Zhu and W. Zhu, *Tetrahedron*, 2015, **71**, 463.

24 R. Chico, C. Domínguez, B. Donnio, B. Heinrich, S. Coco and P. Espinet, *Cryst. Growth Des.*, 2016, **16**, 6984.

25 C. Cuerva, M. Cano and C. Lodeiro, *Chem. Rev.*, 2021, **121**, 12966.

26 M. Bardají and S. Coco, *Organometallic Metallomesogens, in Comprehensive Organometallic Chemistry IV*, ed.G. Parkin, K. Meyer and D. O'hare, Elsevier, Oxford, UK, 2022, vol. 14, ch. 14.09, p. 285.

27 E. Beltran, M. Garzoni, B. Feringan, A. Vancheri, J. Barbera, J. L. Serrano, G. M. Pavan, R. Gimenez and T. Sierra, *Chem. Commun.*, 2015, **51**, 1811.

28 Y. Xiao, X. Su, L. Sosa-Vargas, E. Lacaze, B. Heinrich, B. Donnio, D. Kreher, F. Mathevet and A.-J. Attias, *CrystEngComm*, 2016, **18**, 4787.

29 S. P. Gupta, M. Gupta and S. K. Pal, *ChemistrySelect*, 2017, **2**, 6070.

30 B. Feringan, P. Romero, J. L. Serrano, C. L. Folcia, J. Etxebarria, J. Ortega, R. Termine, A. Golemme, R. Gimenez and T. Sierra, *J. Am. Chem. Soc.*, 2016, **138**, 12511.

31 H. Hayashi, W. Nihashi, T. Umeyama, Y. Matano, S. Seki, Y. Shimizu and H. Imahori, *J. Am. Chem. Soc.*, 2011, **133**, 10736.

32 Y. Xiao, X. Su, L. Sosa-Vargas, E. Lacaze, B. Heinrich, B. Donnio, D. Kreher, F. Mathevet and A. J. Attias, *Cryst. Eng. Commun.*, 2016, **18**, 4787.

33 K.-Q. Zhao, L.-L. An, X.-B. Zhang, W.-H. Yu, P. Hu, B.-Q. Wang, J. Xu, Q.-D. Zeng, H. Monobe, Y. Shimizu, B. Heinrich and B. Donnio, *Chem. – Eur. J.*, 2015, **21**, 10379.

34 A. Kira, T. Umeyama, Y. Matano, K. Yoshida, S. Isoda, J. K. Park, D. Kim and H. Imahori, *J. Am. Chem. Soc.*, 2009, **131**, 3198.

35 T. Umeyama, N. Tezuka, F. Kawashima, S. Seki, Y. Matano, Y. Nakao, T. Shishido, M. Nishi, K. Hirao, H. Lehtivuori, N. V. Tkachencko, H. Lemmetyinen and H. Imahori, *Angew. Chem., Int. Ed.*, 2011, **50**, 4615.

36 E. Tritto, R. Chico, G. Sanz-Enguita, C. L. Folcia, J. Ortega, S. Coco and P. Espinet, *Inorg. Chem.*, 2014, **53**, 3449.

37 A. B. Miguel–Coello, M. Bardají, S. Coco, B. Donnio, B. Heinrich and P. Espinet, *Inorg. Chem.*, 2018, **57**, 4359.

38 E. Tritto, R. Chico, J. Ortega, C. L. Folcia, J. Etxebarria, S. Coco and P. Espinet, *J. Mater. Chem. C*, 2015, **3**, 9385.

39 R. Chico, E. de Domingo, C. Domínguez, B. Donnio, B. Heinrich, R. Termine, A. Golemme, S. Coco and P. Espinet, *Chem. Mater.*, 2017, **29**, 7587.

40 E. de Domingo, C. L. Folcia, J. Ortega, J. Etxebarria, R. Termine, A. Golemme, S. Coco and P. Espinet, *Inorg. Chem.*, 2020, **59**, 10482.

41 M. Barcenilla, M. J. Baena, B. Donnio, B. Heinrich, L. Gutiérrez, S. Coco and P. Espinet, *J. Mater. Chem. C*, 2022, **10**, 9222.

42 P. Cheng, D. Wang and P. Schaaf, *Adv. Sustainable Syst.*, 2022, **6**, 2200115.

43 Y. Xu, S. Wang, Z. Chen, R. Hu, S. Li, Y. Zhao, L. Liu and J. Qu, *J. Nanobiotechnol.*, 2021, **19**, 37.

44 H. Pan, S. Li, J.-L. Kan, L. Gong, C. Lin, W. Liu, D. Qi, K. Wang, X. Yan and J. Jiang, *Chem. Sci.*, 2019, **10**, 8246.

45 Y. Duo, G. Luo, Z. Li, Z. Chen, X. Li, Z. Jiang, B. Yu, H. Huang, Z. Sun and X.-F. Yu, *Small*, 2021, **17**, 2103239.

46 X. Zhang, M. Liu, Z. Kang, B. Wang, F. Jiang, X. Wang, D.-P. Yang and R. Luque, *Chem. Eng. J.*, 2020, **388**, 124304.

47 J. Pan, Y. Guan, Y. Zhang, Z. Xu, S. Han, H. Tang, X. Yan, H. Liu and Q. Lu, *Inorg. Chem.*, 2023, **62**, 624.

48 G. M. Neelgund and A. Oki, *Mater. Chem. Front.*, 2018, **2**, 64.

49 Y. K. Maurya, P. J. Chmielewski, J. Cybińska, B. Prajapati, T. Lis, S. Kang, S. Lee, D. Kim and M. Stępień, *Adv. Sci.*, 2022, **9**, 2105886.

50 S. Vikneshvaran, J. W. Jang, N. N. T. Pham, S. J. Park, G. Balamurugan, S. G. Lee and J. S. Park, *Dyes Pigm.*, 2022, **203**, 110321.

51 H.-H. Wang, J.-Z. Li, J. Nie, Z.-X. Yao, H.-J. Li, K.-G. Liu and X.-W. Yan, *Inorg. Chim. Acta*, 2021, **514**, 120018.

52 H. K. Bisoyi, A. M. Urbas and Q. Li, *Adv. Opt. Mater.*, 2018, **6**, 1800458.

53 F. Camerel and M. Fourmigué, *Eur. J. Inorg. Chem.*, 2020, 508.

54 K. Mebrouk, F. Camerel, O. Jeannin, B. Heinrich, B. Donnio and M. Fourmigue, *Inorg. Chem.*, 2016, **55**, 1296.

55 A. M. Giroud and U. T. Mueller-Westerhoff, *Mol. Cryst. Liq. Cryst., Lett. Sect.*, 1977, **41**, 11.

56 H. Horie, A. Takagi, H. Hasebe, T. Ozawa and K. Ohta, *J. Mater. Chem.*, 2001, **11**, 1063.

57 S. Debnath, H. F. Srour, B. Donnio, M. Fourmigué and F. Camerel, *RSC Adv.*, 2012, **2**, 4453.

58 R. Perochon, L. Piekara-Sady, W. Jurga, R. Clérac and M. Fourmigué, *Dalton Trans.*, 2009, 3052.

59 D. Markovitsi, A. Germain, P. Millié, P. Lécuyer, L. K. Gallos, P. Argyrakis, H. Bengs and H. Ringsdorf, *J. Phys. Chem.*, 1995, **99**, 1005.

60 S. Marguet, D. Markovitsi, P. Millié, H. Sigal and S. Kumar, *J. Phys. Chem. B*, 1998, **102**, 4697.

61 Q. Miao, J. Gao, Z. Wang, H. Yu, Y. Luo and T. Ma, *Inorg. Chim. Acta*, 2011, **376**, 619.

62 D. Markovitsi, A. Germain, P. Millie, P. Lecuyer, L. K. Gallos, P. Argyrakis, H. Bengs and H. Ringsdorf, *J. Phys. Chem.*, 1995, **99**, 1005.

12340 | *J. Mater. Chem. C*, 2024, **12**, 12332–12340

This journal is © The Royal Society of Chemistry 2024